Engineering xxx (xxxx) xxx

Contents lists available at ScienceDirect

Engineering

journal homepage: www.elsevier.com/locate/eng

Research
Environmental Engineering—Article

Unveiling the Mechanism Underlying the Effects of Ammonia on *n*-Caproate Production: Influenced Pathways, Key Enzymes, and Microbiota Functions

Qing-Lian Wu [a,b], Ke-Xin Yuan [a], Wei-Tong Ren [a], Lin Deng [a], Hua-Zhe Wang [a], Xiao-Chi Feng [c], He-Shan Zheng [d], Nan-Qi Ren [a], Wan-Qian Guo [a,*]

[a] *State Key Laboratory of Urban Water Resource and Environment, Harbin Institute of Technology, Harbin 150090, China*
[b] *College of Architecture and Environment, Sichuan University, Chengdu 610065, China*
[c] *State Key Laboratory of Urban Water Resource and Environment, School of Civil and Environmental Engineering, Harbin Institute of Technology (Shenzhen), Shenzhen 518055, China*
[d] *College of Chemistry and Chemical Engineering, Qiqihar University, Qiqihar 161006, China*

ARTICLE INFO

Article history:
Available online xxxx

Keywords:
Ammonia inhibition
Medium chain fatty acids
n-caproate
Enzyme
Metagenomics

ABSTRACT

n-caproate, which is produced via chain elongation (CE) using waste biomass, can supply various fossil-derived products, thus advancing the realization of carbon neutrality. Ammonia released from the degradation of nitrogen-rich waste biomass can act as a nutrient or an inhibitor in anaerobic bioprocesses, including CE, with the distinction being primarily dependent on its concentration. Currently, the optimal concentration of ammonia and the threshold of toxicity for open-culture *n*-caproate production using ethanol as an electron donor, along with the underlying mechanisms, remain unclear. This study revealed that the optimal concentration of ammonia for *n*-caproate production was 2 g·L^{-1}, whereas concentrations exceeding this threshold markedly suppressed the CE performance. Exploration of the mechanism revealed the involvement of two forms of ammonia (i.e., ammonium ions and free ammonia) in this inhibitory behavior. High ammonia levels (5 g·L^{-1}) induced excessive ethanol oxidation and suppressed the reverse β-oxidation (RBO) process, directly leading to the enhanced activities of enzymes (phosphotransacetylase and acetate kinase) responsible for acetate formation and diminished activities of butyryl-coenzyme A (CoA): acetyl-CoA transferase, caproyl-CoA: butyryl-CoA transferase, and caproyl-CoA: acetyl-CoA transferase that are involved in the syntheses of *n*-butyrate and *n*-caproate. Furthermore, the composition of the microbial community shifted from *Paraclostridium* dominance (at 0.1 g·L^{-1} ammonia) to a co-dominance of *Fermentimonas*, *Clostridium sensu stricto* 12, and *Clostridium sensu stricto* 15 at 2 g·L^{-1} ammonia. However, these CE-functional bacteria were mostly absent in the presence of excessive ammonia (5 g·L^{-1} ammonia). Metagenomic analysis revealed the upregulation of functions such as RBO, fatty acid synthesis, K^+ efflux, adenosine triphosphatase (ATPase) metabolism, and metal cation export in the presence of 2 g·L^{-1} ammonia, collectively contributing to enhanced *n*-caproate production. Conversely, the aforementioned functions (excluding metal cation export) and K^+ influx were suppressed by excessive ammonia, undermining both ammonia detoxification and *n*-caproate biosynthesis. The comprehensive elucidation of ammonia-driven mechanisms influencing *n*-caproate production, as provided in this study, is expected to inspire researchers to devise effective strategies to alleviate ammonia-induced inhibition.

1. Introduction

Medium-chain fatty acids (MCFAs) represent valuable platform chemicals generated through chain elongation (CE) technology employing open microbial consortia cultures. They hold immense potential for replacing a portion of fossil fuel-derived products, thereby contributing significantly to the reduction of carbon emissions [1,2]. Furthermore, the enhanced efficiency of MCFAs extraction, driven by advancements in separation and extraction technology, makes industrial applications of MCFAs increasingly feasible [3]. Among these MCFAs, *n*-caproate stands out as one of

* Corresponding author.
E-mail address: guowanqian@126.com (W.-Q. Guo).

https://doi.org/10.1016/j.eng.2023.08.018
2095-8099/

Please cite this article as: Q.-L. Wu, K.-X. Yuan, W.-T. Ren et al., Unveiling the Mechanism Underlying the Effects of Ammonia on *n*-Caproate Production: Influenced Pathways, Key Enzymes, and Microbiota Functions, Engineering, https://doi.org/10.1016/j.eng.2023.08.018

the most prevalent and versatile, used in the production of pharmaceuticals, fragrances, lubricants, rubbers, dyes [4,5], and a key component in the manufacturing of liquid biofuels, including diesel [6] and aviation fuel [7]. The global market demand for *n*-caproate is exhibiting remarkable growth, projected to reach an approximate value of eight billion USD by 2023 [8]. Striking a harmonious balance between economic viability and environmental sustainability underscores the unanimous endorsement of using waste biomass as the primary feedstock [4]. However, several available waste biomass sources, such as brewing wastewater [9,10], food waste [11], excess sludge [12], and livestock manure [13], inherently contain high nitrogen content. This characteristic leads to the release of ammonia, comprising ammonium ions (NH_4^+) and free ammonia (FA), during substrate biodegradation. At elevated concentrations, ammonia can pose a significant hindrance to microbial activity [14]. As a result, several anaerobic reactors operate under conditions triggered by ammonia, thereby diminishing CE performance and stability. Understanding the impacts and underlying mechanisms of ammonia-induced inhibition is essential for developing effective strategies to enhance *n*-caproate production. Importantly, the response of *n*-caproate-producing bacteria to ammonia inhibition may significantly differ from that of other anaerobic bacteria, such as methanogens, necessitating further research in this area.

Until now, scant attention has been directed toward investigating the implications of ammonia on *n*-caproate production. A crucial distinction arises between *n*-caproate production and methane/hydrogen production, primarily because undissociated *n*-caproate (*n*-caproic acid) itself exerts toxicity on bacteria [4]. Microbial activity is significantly suppressed at an *n*-caproic acid concentration of 3.3 mmol·L^{-1} [15], and severe inhibition occurs at 6.9 mmol·L^{-1}, affecting the conversion of acetate and *n*-butyrate to *n*-caproate [16]. Additionally, the intermediates of short-chain fatty acids (SCFAs) also act as inhibitors, with their toxic effects intensifying as the carbon chain lengthens [3]. Consequently, the accumulation of both intermediate and end products can disrupt the micro-ecosystem and microbial activity. When combined with the presence of ammonia, this dynamic could create a dual inhibitory effect on the CE process. Thus, it is plausible that the threshold for ammonia inhibition in CE reactors may be notably lower than in other anaerobic reactors. In CE, two frequently employed electron donors are ethanol and lactate, and their principal metabolic divergence arises from the electron donor oxidation phase [1]. For instance, Zhang et al. [17] reported a 2.1 g·L^{-1} ammonia inhibition threshold for the *n*-caproate-producing strain *Clostridium kluyveri* DSM 555 when ethanol served as the electron donor. Wei et al. [18] revealed that 1–4 g·L^{-1} ammonia linearly decreased *n*-caproate production by 25%–80% in the *Clostridium* Ⅳ-dominated CE reactor where food waste was utilized as a substrate, with lactate as an intermediate and electron donor. Nevertheless, to our knowledge, comprehensive research regarding the effect of ammonia on open culture *n*-caproate production when ethanol is employed as the electron donor remains scarce. Moreover, the intricate mechanisms underlying the effects of both stimulatory and inhibitory ammonia concentrations on open culture *n*-caproate production remain to be adequately elucidated.

Consequently, this study aims to achieve two primary objectives: firstly, to investigate the influence of varying ammonia concentrations on open-culture *n*-caproate production when ethanol is utilized as the electron donor; and secondly, to uncover the intrinsic mechanisms underlying the effects of ammonia on *n*-caproate production. This comprehensive investigation encompasses four distinct dimensions: ① identifying the form of ammonia responsible for inducing inhibitory behavior; ② revealing how ammonia impacts the two critical stages of CE (i.e., ethanol oxidation and reverse β-oxidation (RBO)), along with the corresponding key enzyme activities; ③ identifying the response of microbial communities to different ammonia concentrations; ④ elucidating the influence of ammonia on microbiota functions.

2. Materials and methods

2.1. Inoculum and media

The inoculum used in this study was waste-activated sludge collected from the sedimentation tank of the Wenchang Wastewater Treatment Plant (China). The sludge was filtered using a 1 mm screen to eliminate impurities and concentrated by settling at 4 °C for 24 h, obtaining the final properties: total suspended solid (TSS) of 16.81 g·L^{-1}, volatile suspended solid (VSS) of 10.93 g·L^{-1}, total chemical oxygen demand (COD) of 16.38 g·L^{-1}, soluble COD of 0.58 g·L^{-1}, and pH of 6.72. The anaerobic fermentation medium composition (per liter) included 0.2 g $MgSO_4·7H_2O$, 0.23 g KH_2PO_4, 0.31 g K_2HPO_4, 0.8 g NaCl, 0.25 g L-cysteine-HCl·H_2O, 10 g 2-bromoethanesulfonate (methanogens inhibitor), 1 mL vitamin solution, and 1 mL trace-element solution. The components of the vitamin and trace-element solutions were obtained from our previous study [9].

2.2. Effects of ammonia concentrations on MCFAs production performance

The experiments were conducted in 21 identical anaerobic reactors (working volume of 250 mL) belonging to seven groups with three parallel samples each. The inoculum (25 mL), medium (100 mL), and substrates (150 mmol·L^{-1} ethanol + 50 mmol·L^{-1} acetate) were added to each reactor. To attain the desired ammonia concentrations, NH_4Cl was introduced into the seven groups, resulting in concentrations of 0.1, 0.5, 1, 2, 3, 4, and 5 g·L^{-1}. Because ammonia below 0.2 g·L^{-1} is uninhibited and is usually used in anaerobic fermentation [19], the group treated with 0.1 g·L^{-1} ammonia was labeled as the control. Moreover, a reactor consisting of only 25 mL of the inoculum and 100 mL of distilled water was considered a blank to exclude MCFAs generated from the inoculum. The initial pH of each reactor was adjusted to 6.5. All reactors were ultimately flushed with N_2 (99.9%) for 5 min and stirred in an air-bath shaker (35 °C, 120 r·min^{-1}).

2.3. Effects of ammonia on ethanol oxidation and RBO stages

The experiments were conducted in six replicate serum bottles (working volume of 50 mL, three in parallel), and divided into groups I and II to investigate the effect of ammonia on ethanol oxidation and RBO, respectively. The 5 mL of the inoculum and 20 mL of the medium were added to each serum bottle. NH_4Cl was added to the reactors of these two groups to produce ammonia at concentrations of 0.1, 2, and 5 g·L^{-1}. Subsequently, 150 mmol·L^{-1} of ethanol was added to each bottle in group I as the sole substrate. The 3 mmol·L^{-1} acetyl-coenzyme A (CoA) (Sigma-Aldrich Corporation, USA), 3 mmol·L^{-1} acetate, and 1 mmol·L^{-1} adenosine triphosphate (ATP) (Sigma-Aldrich Corporation) were added to each bottle in group Ⅱ as substrates. Finally, all serum bottles were operated for six days under the same conditions as described in Section 2.2. The fermentation liquor was removed on day 2, 4, and 6 to measure the changes in the concentrations of ethanol, acetyl-CoA, SCFAs, and MCFAs.

2.4. Effects of ammonia on the activity of key enzymes in the CE process

Cell extracts from the reactors with 0, 2, and 5 g·L^{-1} ammonia in Section 2.2 were prepared to assay relevant enzyme activities using the following procedure. The sludge (30 mL) was procured from the specific anaerobic reactor, centrifuged at 8000 r·min^{-1} and 4 °C for 10 min, and washed with 0.05 mol·L^{-1} tris(hydroxyme thyl)aminomethane HCl (Tris-HCl) buffer (pH = 6.5). This process was repeated three times, and the centrifuged sludge was resuspended in 20 mL of Tris-HCl buffer. Then, the suspended sludge was ultrasonically crushed (30 kHz) under an ice–water bath for 20 min, and centrifuged at 10 000 r·min^{-1} and 4 °C for 30 min to remove cell debris. The resulting supernatant was used as the cell extract. The activity of enzymes involved in the ethanol oxidation (i.e., alcohol dehydrogenase (Adh), aldehyde dehydrogenase (Ald), phosphotransacetylase (Pta), and acetate kinase (Ak)) was determined via reference to previous studies [20–22]. The activities of key enzymes relevant to RBO, including butyryl-CoA: acetyl-CoA transferase (BCoAT), caproyl-CoA: butyryl-CoA transferase (Cbt), and caproyl-CoA: acetyl-CoA transferase (Cat) were measured as described by Wei et al. [18] and Zhu et al. [23]. The specific enzyme activity was calculated as units (U) per milligram of VSS.

2.5. Microbial community and metagenomic sequencing analysis

The three reactors with 0.1, 2, and 5 g·L^{-1} ammonia were semi-continuously operated for 30 d, and microbial samples were collected every 10 d to measure the microbial community. DNA was extracted using an E.Z.N.A^{TM} Mag-Bind Soil DNA Kit (Omega Biotek, USA). Polymerase chain reaction amplification of the V4 region of the 16S ribosomal RNA gene was performed using primers 515F and 806R. Sequencing libraries were constructed, and paired-end sequencing was performed using the Illumina MiSeq platform at Majorbio Co., Ltd. (China). Clean sequences were clustered into operational taxonomic units (OTUs) with a 97% similarity threshold using UPARSE (version 7.0.1090). The taxonomy of each OTU sequence was analyzed using the ribosomal database project classifier.

Metagenome sequencing was conducted based on the extracted DNA at a sequencing depth of 6 Gbase. The DNA extract was fragmented to an average size of ~300 base pair (bp) using a Covaris M220 (Gene Co., Ltd., China) for paired-end library construction using the TruSeq DNA Sample Preparation Kit (Illumina Corporation, USA) by Majorbio Bio-Pharm Technology Co., Ltd. (China). Paired-end sequencing was performed using the Illumina HiSeq4000 platform. Fastp software (v0.20.0) was used for quality control of the raw sequencing data. Metagenomic data were assembled using MEGAHIT (v1.1.2). Contigs with a length $\geq$ 300 bp were selected as the final assembling result. The open reading frames (ORFs) were predicted using Prodigal (v2.6.3), and the number of ORFs collected for the control, 2, and 5 g·L^{-1} groups were 774 354, 580 690, and 851 150, respectively. CD-HIT software (v4.6.1) was used to cluster genetic data with 95% sequence identity (90% coverage). From each cluster, the longest sequences were selected as representative sequences to construct a non-redundant gene catalogue, which were aligned to the non-redundant protein sequence database with an e-value cutoff of 1×10^{-5}. The high-quality reads of each sample were compared with the non-redundant gene set (95% identity) using the SOAPaligner software. Gene abundance was calculated with transcripts per million based on the mapped reads. The Kyoto Encyclopedia of Genes and Genomes (KEGG) annotation was conducted using Diamond (v0.8.35) to compare the non-redundant gene catalogue with KEGG database with an e-value cutoff of 1×10^{-5}. The relative abundances of functional genes encoding enzymes were calculated, and compared to assess the functions and metabolic pathways influenced by different ammonia concentrations.

2.6. Analytic methods

Ethanol, SCFAs, and MCFAs were analyzed using a gas chromatograph (7890; Agilent Technologies, USA) equipped with a flame ionization detector and a 30 m × 0.25 mm DB WAX polyethylene glycol capillary column. The inlet and detector temperatures were 220 and 240 °C, respectively. The column temperature program increased the temperature from an initial 70 to 170 °C with a temperature ramp of 20 °C·min^{-1}, and maintained at 170 °C for 5 min followed by a temperature ramp of 20 °C·min^{-1} to 240 °C. Their concentrations were converted to COD values using the established conversion factors [9].

Selectivity was used to estimate the conversion rate of the substrate into MCFAs, which was calculated by dividing the electron equivalents of the products by the consumed electrons from the participant substrates [10]. Carbon flow distribution, expressed as a percentage, indicates the proportion of the molar concentration of carbon in the product relative to the substrate used. TSS, VSS, COD, and ammonia concentrations were measured according to Standard Methods (APHA, 2005). pH was measured using a pH probe (PHS-3E; LeiCi Corporation, China). The FA concentration was calculated using Eq. (1) [24].

$$A = \frac{TAN}{1 + \frac{10^{-pH}}{K_a}} \quad (1)$$

Where TAN is the total concentration of FA and NH_4^+, mg·L^{-1}; K_a indicates the dissociation constant, which is 1.13×10^{-9} at 35 °C.

Principal component analysis (PCA) was performed to estimate the discrepancies and similarities between different microbiomes. The linear discriminant effect size (LEfSe) was used to identify key discriminative microbial taxa, and the corresponding linear discriminant analysis (LDA) values were used to quantitatively evaluate the degree of influence. The Student's t-test was used to evaluate significant differences at the bacterial genus level.

3. Results and discussion

3.1. Influences of the concentration of ammonia on n-caproate production

Fig. 1 demonstrates the substrate utilization, *n*-caproate production, product selectivity, and carbon flow distribution under different ammonia concentrations. The production of *n*-caproate was significantly enhanced at 0.5–2.0 g·L^{-1} ammonia compared with the control, indicating that the ammonia concentration required for *n*-caproate generation may be higher than the usual concentration (< 0.2 g·L^{-1}). The highest *n*-caproate production of 10.88 g·L^{-1} and selectivity of 67.82% were obtained with 2.0 g·L^{-1} of ammonia, which were approximately 44.49% and 44.48% higher than those obtained from the control, respectively. However, *n*-caproate production was significantly reduced at ammonia concentrations > 2.0 g·L^{-1}, which was lower than that at the control. In particular, *n*-caproate selectivity was as low as 5.96% at 5.0 g·L^{-1} ammonia. Furthermore, the substrate–carbon flow to *n*-caproate reached approximately 70% at 2.0 g·L^{-1} ammonia; however, it sharply dropped with increasing ammonia concentration. Therefore, both the optimal ammonia concentration and inhibitory threshold were 2.0 g·L^{-1}. Similarly, Zhang et al. [17] reported an ammonia threshold of 2.1 g·L^{-1} for the CE strain *Clostridium kluyveri* with ethanol as an electron donor. However, Wei et al. [18] revealed that *n*-caproate synthesis was suppressed when the ammonia concentration exceeded 1 g·L^{-1} in cases where

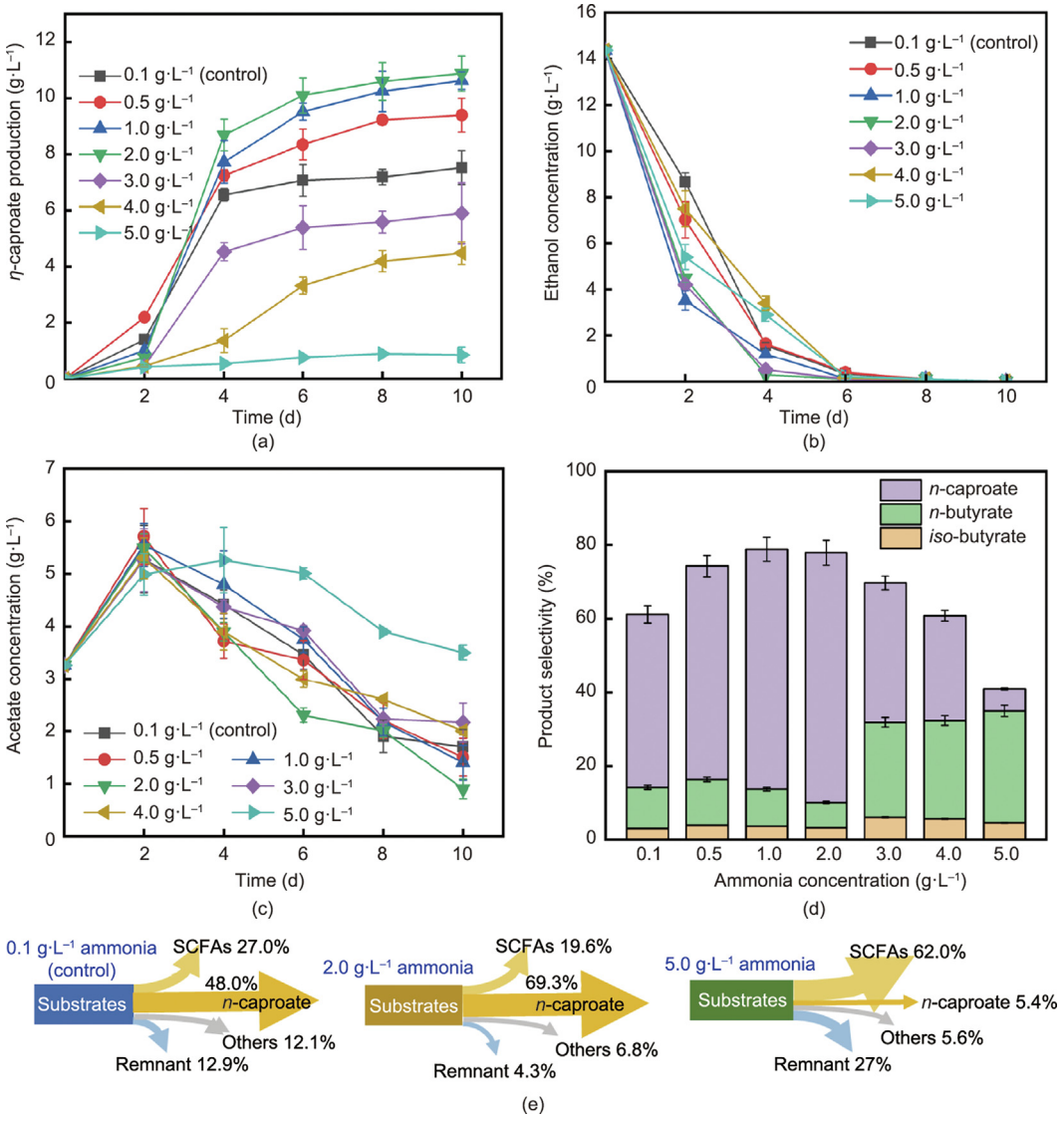

Fig. 1. Effect of ammonia concentrations on *n*-caproate production performance: variations of the concentrations of (a) *n*-caproate, (b) ethanol, and (c) acetate with time; and the differences in (d) product selectivity and (e) carbon flow distribution.

lactate was used as an electron donor. These observations indicate that microbial communities utilizing ethanol as an electron donor may be more resistant to ammonia, which might be attributed to the lower inhibition of ethanol oxidation by ammonia than lactate oxidation (the first stage of CE). This conjecture is based on ethanol utilization, as shown in Fig. 1(b). Almost all ethanol was quickly utilized under 0.1–5.0 g·L^{-1} ammonia within 6 d, whereas lactate utilization was reported to be significantly slowed at 2–4 g·L^{-1} ammonia and even suspended at 5–6 g·L^{-1} ammonia [18]. Furthermore, excessive ammonia produced more SCFA residues, suggesting that excessive ammonia could limit the RBO stage that converts SCFAs.

3.2. Effects of ammonia on the two stages of CE

The effect of ammonia on ethanol oxidation and RBO was investigated to determine the specific inhibitory pathways. As shown in Figs. 2(a)–(c), ethanol as the sole substrate was quickly consumed without a noticeable difference among the control, 2 g·L^{-1} ammonia, and 5 g·L^{-1} ammonia groups; however, a significant difference was observed in the products. At 2 g·L^{-1} ammonia, acetate production was similar to that of the control, along with the highest acetyl-CoA concentration. However, the acetate concentration reached the highest level, whereas the acetyl-CoA concentration was the lowest in the whole process under 5 g·L^{-1} ammonia. On day 4, *n*-butyrate was detected, and its concentration trend was almost opposite to that of acetate (Fig. 2(d)). It was indicated that excessive ammonia may stimulate the excessive ethanol oxidation (EEO) for the generation of acetate ($C_2H_6O + H_2O \rightarrow C_2H_3O_2^- + H^+ + 2H_2$) that is performed by ethanol-oxidizing microorganisms, which do not perform CE [25], resulting in the deficiency of acetyl-CoA. Therefore, although ethanol utilization was not inhibited by excessive ammonia, the ethanol conversion pathway may differ from that at low ammonia.

When acetyl-CoA and acetate were fed as substrates, acetyl-CoA was quickly utilized by the bacteria, and was almost undetectable in the fermentation broth from day 2 in all three groups (Fig. 2(e)). The acetate concentration increased slightly with time under 5 g·L^{-1} ammonia (Fig. 2(f)); however, almost no *n*-butyrate and *n*-caproate were detected (Figs. 2(g) and (h)), indicating that acetyl-CoA may be converted to acetate but did not elongate acetate. In contrast, acetate was utilized, and *n*-butyrate and *n*-

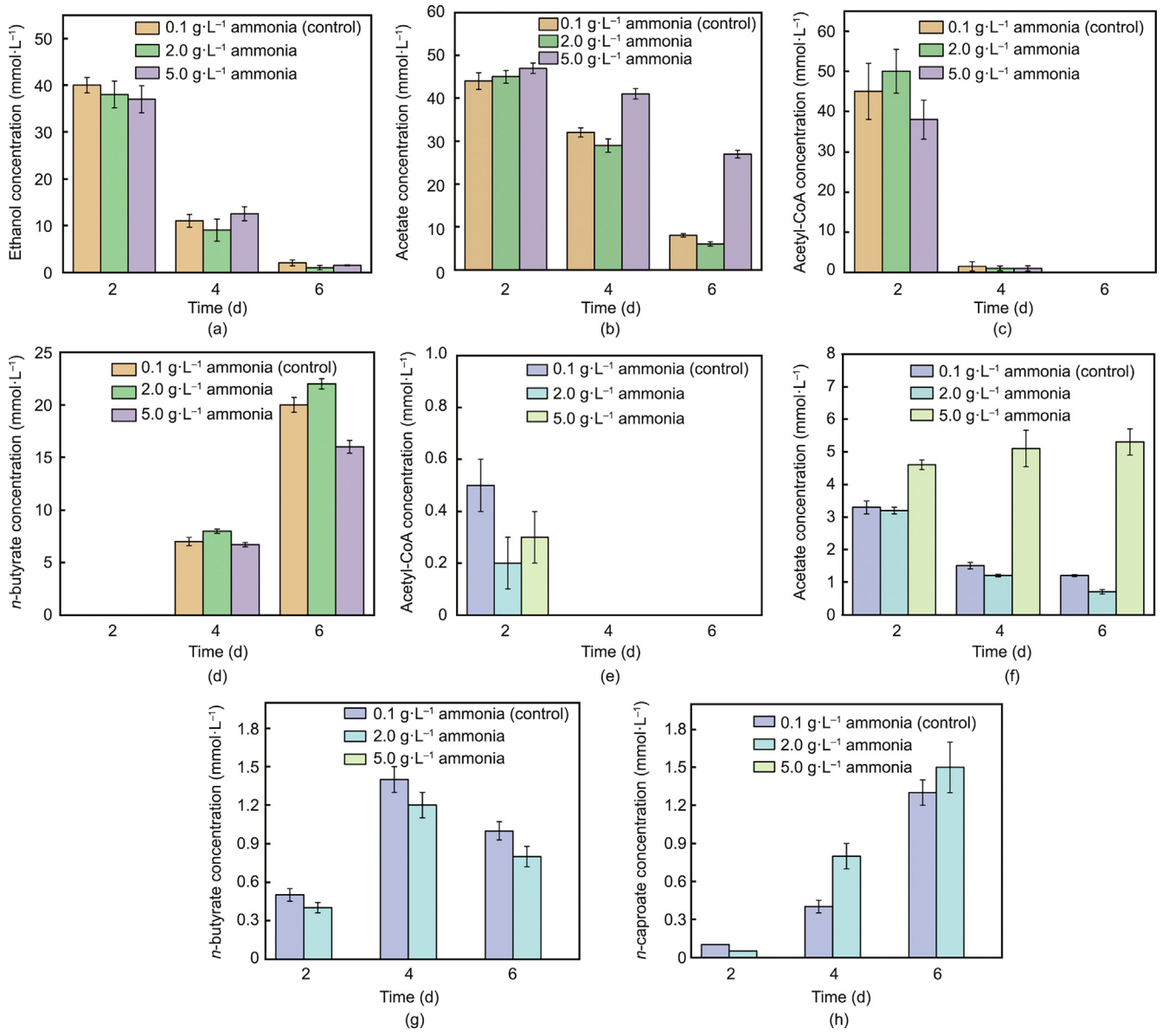

Fig. 2. Effects of ammonia on ethanol oxidation, RBO processes, and the related enzyme activities. Variations of (a) ethanol, (b) acetate, (c) acetyl-CoA, and (d) *n*-butyrate concentrations in the ethanol oxidation process; and (e) acetyl-CoA, (f) acetate, (g) *n*-butyrate, and (h) *n*-caproate concentrations in the RBO process.

caproate were produced in the control and 2 g·L^{-1} ammonia reactors, respectively. Therefore, excessive ammonia not only limited acetyl-CoA generation from ethanol oxidation, but also inhibited the elongation of SCFAs via the RBO pathway.

3.3. The form of ammonia that produces an inhibitory effect

The inhibitory effect of ammonia on anaerobic microorganisms is associated with the two forms, NH_4^+ and FA. Among them, FA is generally considered to be the primary inhibitor that diffuses freely into microbial cells to cause physiological dysfunction [14], and its concentration primarily depends on temperature, pH, and total ammonia concentration [26]. The variations in pH and FA concentration at 37 °C are shown in Fig. S1 in Appendix A. With the conversion of ethanol to fatty acids, the pH first decreased and then stabilized, and the FA/NH_4^+ equilibrium varied with the concentration of ammonia. It was observed that FA concentrations were < 4 mg·L^{-1} and 4–10 mg·L^{-1} in the uninhibited (0.1–2 g·L^{-1} ammonia) and inhibited (3–5 g·L^{-1} ammonia) reactors, respectively. To confirm whether low FA content inhibited *n*-caproate generation, we lowered the initial pH to 6 to reduce the concentration of FA. Variations in pH, FA concentration, and *n*-caproate concentration are shown in Fig. S2 in Appendix A. Comparing Fig. S2 with Fig. 1, it was observed that the decreased pH resulted in a lower FA concentration, which could have also affected the inhibitory concentration of ammonia. For instance, in the reactor with 3 g·L^{-1} ammonia, the FA concentrations at the initial pH = 6 and 6.5 were 0.7–1.7 mg·L^{-1} and 3.1–5.7 mg·L^{-1}, respectively; and *n*-caproate production was slightly enhanced compared to that of the control at the lower pH of 6, indicating that the decreased FA concentration mitigated the inhibitory effect. The FA inhibitory concentration (> 3 mg·L^{-1}) observed in this study was lower than the reported inhibition thresholds (> 10 mg·L^{-1}) for anaerobic fermentation [26–28]. A possible explanation for this is that the presence of multiple inhibitors (including ammonia and undissociated fatty acids) decreased the respective inhibitory thresholds. Therefore, the MCFAs production process requires stricter control of ammonia than other anaerobic processes.

Furthermore, the maximum FA concentration at pH = 6 in the inhibited reactors (4 and 5 g·L^{-1} ammonia) was < 3 mg·L^{-1}, suggesting that high NH_4^+ content could be a key inhibitor. NH_4^+ primarily inhibits anaerobes by decreasing the activity of the enzymes involved in microbial metabolism [29]. The activities of crucial enzymes in the CE process were measured to analyze the inhibitory effects of NH_4^+. Adh, Ald, Pta, and Ak were found to be involved in ethanol oxidization [1]. Zhu et al. [23] revealed that BCoAT is specifically responsible for *n*-butyrate generation, and Cbt and Cat are involved in *n*-caproate generation. As shown in Fig. 3(a), the difference in activity between Adh and Ald at the three ammonia levels was not as significant as that between Pta and Ak, and the latter two were enhanced with increasing ammonia concentration, which further confirmed that excessive ammonia facilitated the EEO process. Energy consumption is required for bacteria to balance intracellular protons and pH under ammonia stress [26], which could be the reason for the promoted conversion of acetyl-CoA to acetate because it is an energy-harvesting process. Moreover, compared with the control, the activities of BCoAT, Cbt, and Cat at 2 g·L^{-1} ammonia were further enhanced by approximately 25%, 40%, and 8%, respectively, whereas they were significantly suppressed to the extent that they were nearly undetectable at 5 g·L^{-1} ammonia (Fig. 3(b)), consistent with the difference in *n*-caproate production. As shown in Fig. 3(c), the enzymes mentioned above are involved in key biotransformation pathways of the CE process. Therefore, excess NH_4^+ inhibits the activity of the enzymes directly involved in the synthesis of MCFAs.

3.4. Effects of ammonia on the microbial community

The microbial composition was analyzed to identify the response of microorganisms to various ammonia concentrations. According to the PCA results (Fig. 4(a)), the microbiomes in the control, 2 g·L^{-1} ammonia, and 5 g·L^{-1} ammonia groups were clustered and separated, indicating clear distinctions in the community structures. Ammonia content affected *n*-caproate production, likely by shifting the microbial community structure. Firmicutes, Actinobacteriota, Bacteroidota, Proteobacteria, Chloroflexi, and Desulfobacterota were the major phyla in all the three groups (Figs. S3(a)–(c) in Appendix A). Compared with the control, the relative abundance of Firmicutes decreased, but that of Bacteroidota significantly increased with increasing ammonia content, suggesting a higher ammonia tolerance of Bacteroidota. In contrast, the relative abundance of Actinobacteriota considerably increased at 2 g·L^{-1} ammonia, but decreased at 5 g·L^{-1} ammonia stress. Both Bacteroidota and Actinobacteriota are important phyla involved in MCFA generation [9,30]. Therefore, these two phyla can be considered critical *n*-caproate producers. The three dominant classes, Clostridia, Actinobacteria, and Bacteroidia, underwent similar abundance changes as their affiliated phyla (Figs. S3(d)–(f) in Appendix A).

LEfSe and Student's t-tests were combined to identify the key discriminative microbial taxa and evaluate significant differences between the three groups. As shown in Fig. S4 in Appendix A and Figs. 4(b) and (c), Clostridia (25% at 2 g·L^{-1} and 33% at 5 g·L^{-1}) and Actinobacteria (42% at 2 g·L^{-1} and 11% at 5 g·L^{-1}) were identified as the primary classes at 2 and 5 g·L^{-1} ammonia, respectively. Among these, Clostridia are widely acknowledged to include the most diverse array of *n*-caproate-producing microorganisms [31]. Members of the order Clostridiales and family Clostridiaceae were also discriminated as key bacteria (LDA scores ($\log_{10}$ scale) > 4.5) that distinguished 2 g·L^{-1} ammonia from the others. Furthermore, compared to the control (9%), the relative abundance of *Paraclostridium* showed the most significant difference at 2 g·L^{-1} (2.4%) and 5 g·L^{-1} (3.7%) ammonia. *Paraclostridium* has the same physiological and morphological characteristics as

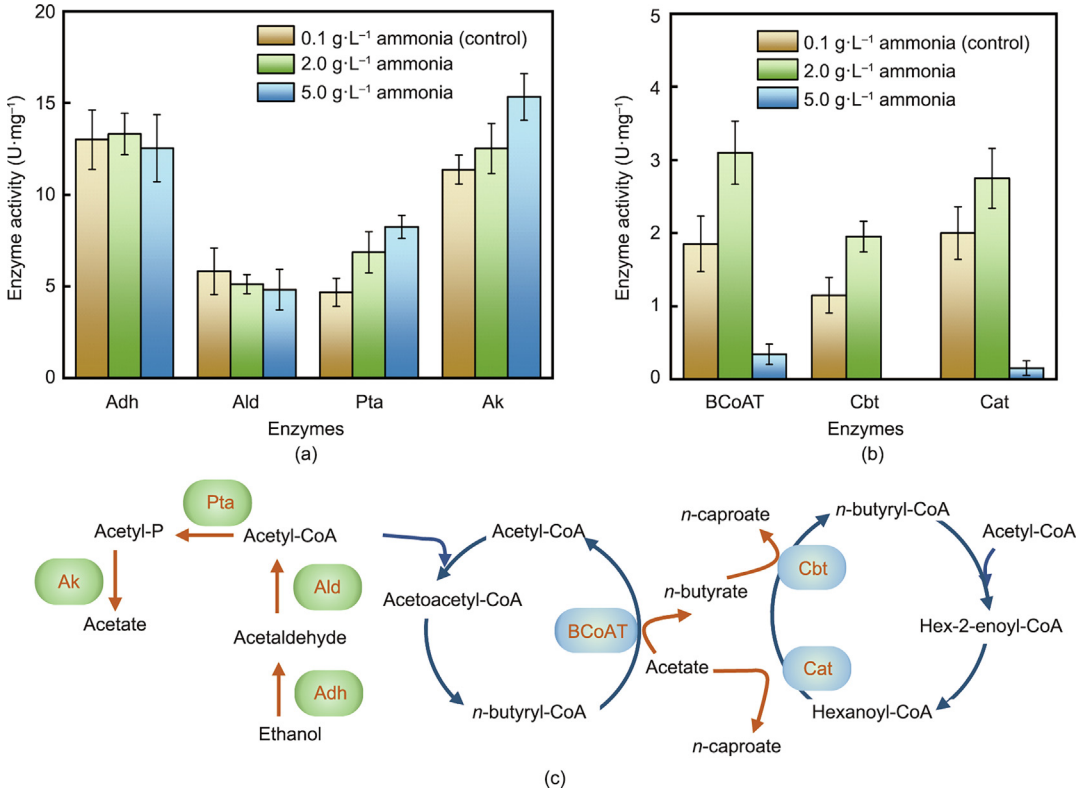

Fig. 3. Activity of the key enzymes related to the processes of (a) ethanol oxidation and (b) RBO, and the (c) schematic diagram of the pathways involving in these enzymes. P: phosphate; Hex: hexanoyl.

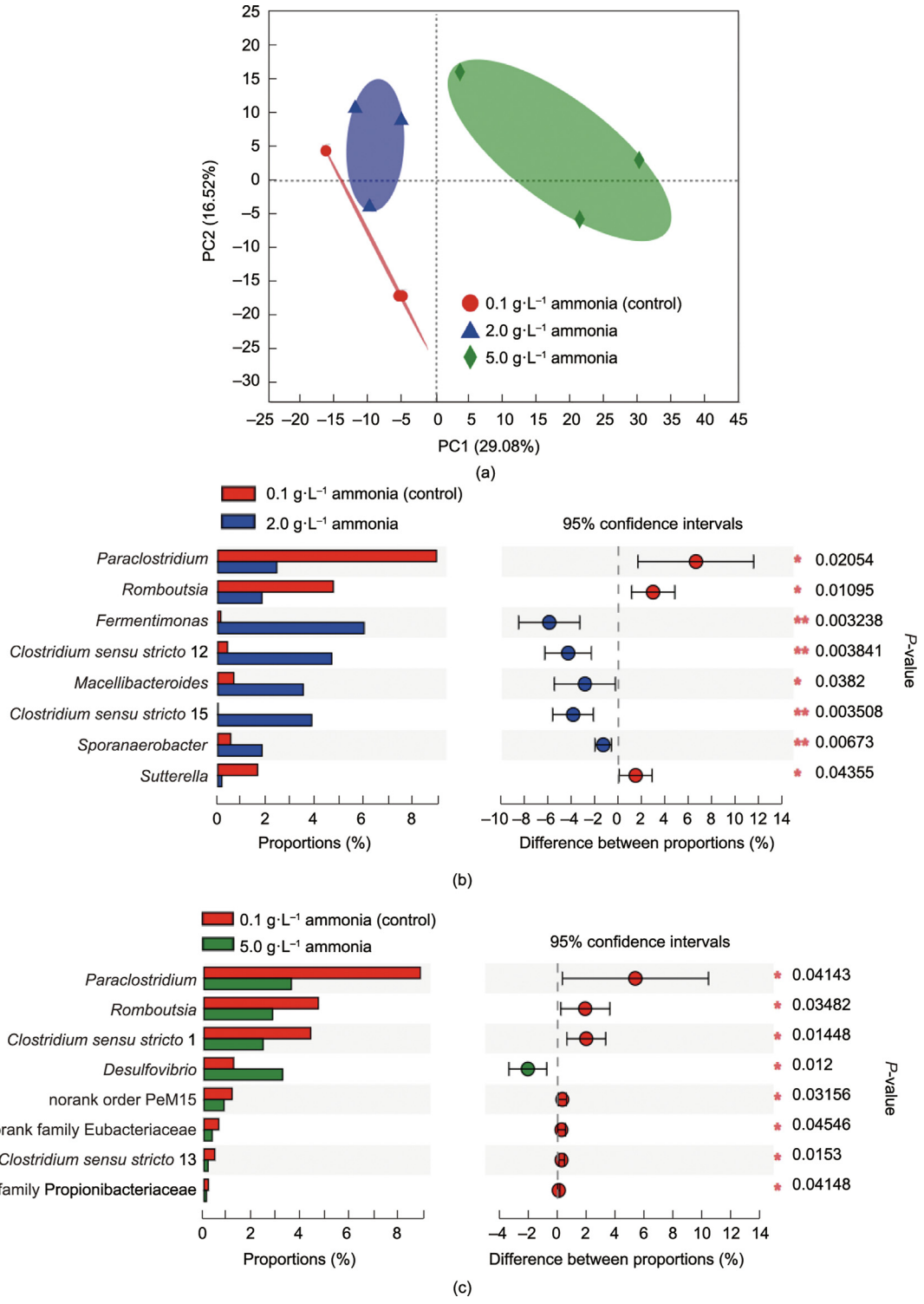

Fig. 4. The difference analysis of microbial communities under different ammonia contents. (a) PCA analysis of the microbiomes from three ammonia contents. Comparison of the microbial community at genus level between (b) control and 2 g·L^{-1} ammonia, and (c) control and 5 g·L^{-1} ammonia, based on Fisher Exact Test at 95% confidence intervals.

Clostridium, and can convert organic substrates into H_2 and *n*-butyrate [32]. Moreover, Zagrodnik et al. [33] and Yin et al. [34] revealed a positive correlation between *n*-caproate production and *Paraclostridium* on ethanol and acetate substrates. Therefore, it was conjectured that *Paraclostridium* mainly participates in the first cycle of RBO for *n*-butyrate synthesis. *Paraclostridium* was the dominant genus in all three groups, but its abundance declined significantly with increasing ammonia content, indicating low ammonia tolerance. In contrast, several ammonia-tolerant CE-related bacteria were enriched, including *Fermentimonas*, *Macellibacteroides*, *Clostridium sensu stricto* 12, *Clostridium sensu stricto* 15, and *Sporanaerobacter*. *Fermentimonas* is an anaerobic acetogen involved in ethanol oxidation [35]. Similarly, *Clostridium sensu stricto* 15 indirectly contributes to *n*-caproate production by con-

verting organics to acetate [36]. *Macellibacteroides* was identified as an *n*-butyrate producer that plays a synergistic role with *Clostridium* in the RBO process [37]. *Clostridium sensu stricto* 12 had been observed in several CE reactors, which was directly related to *n*-caproate production [38–40]. *Sporanaerobacter* can participate in direct interspecies electron transfer [41], which is also significantly and positively correlated with MCFA production [34]. The significant enrichment of these genera at 2 g·L^{-1} ammonia was an important reason for the enhanced *n*-caproate production. However, these genera could not tolerate high ammonia stress (5 g·L^{-1}) and almost no *n*-caproate-producing bacteria were enriched under excessive ammonia. Wei et al. [18] also revealed that CE bacteria were less tolerant of high ammonia levels than propionate-producing bacteria, and the microbial community was reshaped from *Clostridium* IV domination to *Clostridium* IV and *Propionibacterium* co-domination as ammonia increased from 2 to 4 g·L^{-1}.

3.5. Effects of ammonia on the functional traits of microbiota

The metabolic behavior of microorganisms is related to their functional genes [42]. Hence, metagenomic analysis was used to determine the fundamental reason why ammonia shifted the microbial community and affected *n*-caproate production. Figs. 5 (a)–(c) show the relative abundance of functional genes and pathways, the relevant functions promoted or inhibited, and the key processes affected by the ammonia concentration, respectively.

(1) **Ethanol oxidation-related functions.** The efficiency of ethanol oxidation definitively affects *n*-caproate production because it provides energy, reducing equivalents, and the indispensable intermediate acetyl-CoA for *n*-caproate synthesis [3]. As shown in Fig. 5(a), the functional genes *Adh*, *Ald*, and aldehyde–ferredoxin oxidoreductase (*Aor*) are involved in acetyl-CoA generation, and genes *Pta* and *Ak* are involved in the conversion of acetyl-CoA to acetate, increased by 4.25%–54.64% under 2 g·L^{-1} ammonia, compared with the control. Among them, the abundance of genes *Adh* and *Ak* were significantly improved by 13.12% and 31.29%, respectively, whereas the other three genes were almost unchanged at 5 g·L^{-1} ammonia. This indicates that ethanol oxidation was promoted by both ammonia contents, which is consistent with the conclusion of Section 3.2; therefore, ethanol oxidation was ammonia-tolerant. Xing et al. [43] also reported the robustness of ethanol oxidation under an ammonia-toxic dose to methanogens, where the abundance of genes *Adh* and *Aor* increased by 32%. Because transforming acetyl-CoA to acetate is an ATP harvest process [4], the significantly increased abundance of genes encoding this process under 2 and 5 g·L^{-1} ammonia could ensure sufficient energy for subsequent CE. However, increasing the oxidation of acetyl-CoA to acetate, that is, EEO, is not expected to occur in the case of a shortage of acetyl-CoA in the RBO stage [25]. Fortunately, 2 g·L^{-1} ammonia did not induce EEO because acetate and *n*-butyrate were not obviously accumulated. However, acetate accumulation occurred at 5 g·L^{-1} ammonia, which could have been caused by EEO or the attenuated RBO.

(2) **RBO-related functions.** RBO is followed by ethanol oxidation for *n*-caproate synthesis with acetyl-CoA as a 2-carbon donor. As shown in Fig. 5(a), the relative abundance of genes encoding key enzymes in this step differed significantly among the three ammonia contents. First, the abundance of genes acetyl-CoA C-acetyltransferase (*atoB*), which is involved in acetoacetyl-CoA formation to start the first cycle of RBO, was significantly increased by 32.56% but decreased by 46.15% compared to the control under 2 and 5 g·L^{-1} ammonia, respectively. Subsequently, the genes 3-hydroxybutyryl-CoA dehydrogenase (*Hbd*), 3-hydroxybutyryl-CoA dehydratase (*croR*), and electron transport flavoproteins alpha (*etfA*) and beta subunits (*etfB*), which are responsible for butyryl-CoA formation, were increased by 9.78%–48.09% at 2 g·L^{-1} ammonia but reduced by 22.55%–48.53% at 5 g·L^{-1} ammonia. A similar situation occurs with the gene of butyryl-CoA: acetate CoA transferase (*BCoAT*) which catalyzes the conversion of butyryl-CoA and acetate to butyrate and acetyl-CoA [44]. Therefore, excessive ammonia severely inhibits the first cycle of RBO in *n*-butyrate synthesis. In contrast, the optimal ammonia concentration of 2 g·L^{-1} positively promoted it, which directly enhanced *n*-caproate production. Along with the first cycle, excess ammonia inhibited the second and third cycles, which was mainly reflected in the reduced abundance of genes acetyl-CoA acyltransferase-2 (*Acca*), enoyl-CoA hydratase (*Echs*), and acyl-CoA thioesterase (*Te*). Meanwhile, the abovementioned three genes and the genes 3-hydroxyacyl-CoA dehydrogenase (*Hadh*) and trans-2-enoyl-CoA reductase (*Ter*) increased to some degree at 2 g·L^{-1} ammonia. Furthermore, the magnitude of genetic variation in the second and third RBO cycles was not as significant as that in the first cycle. In summary, excess ammonia significantly inhibits RBO, especially in the first cycle, whereas the optimal ammonia dose promotes the entire RBO process.

(3) **Fatty acid synthesis (FAS)-related functions.** In addition to RBO, FAS, an indispensable bioprocess in microorganisms, plays a role in the synthesis of MCFAs as precursors for building phospholipids and sterols [45]. FAS is initiated by a 3-carbon donor, malonyl-CoA, which is produced from the carboxylation of acetyl-CoA and the conversion of malonate catalyzed by acetyl-CoA carboxylase (*Acc*) and acid-thiol ligases (*Atl*), respectively [3]. The abundance of genes encoding *Acc* and *Atl* was upregulated at 2 g·L^{-1} ammonia, but downregulated at 5 g·L^{-1} ammonia. It appears that ammonia affects FAS in a manner similar to that of RBO. However, the expression of other genes encoding FAS enzymes did not change so regularly and significantly. For example, the abundances of genes encoding β-ketoacyl-synthase Ⅱ (*fabF*) and 3-oxoacyl-reductase (*fabG*), involved in the generation of key intermediates, were improved at 2 g·L^{-1} ammonia but reduced at 5 g·L^{-1} ammonia than control. However, genes encoding phosphate butyryltransferase (*fabD*), which is responsible for malonyl-acyl carrier protein generation, 3-hydroxyacyl-dehydratase (*fabZ*), and enoyl-reductase (*fabV*) were reduced at both ammonia concentrations. Furthermore, the relative abundance of genes related to FAS was much lower than that related to RBO, indicating that the genes associated with FAS barely affected *n*-caproate production.

(4) **Potassium transport-related functions.** Under ammonia stress, FA can rapidly diffuse through the cell membrane and absorb H^+ to form NH_4^+, resulting in intracellular pH disturbances and proton imbalance [46]. As a result, microorganisms must activate the K^+ antiporter to pump out K^+ for intracellular proton balance, during which the K^+ transport system, including K^+ influx and efflux, plays a key role [43]. The K^+ influx is primarily regulated by genes *Trk*, *Ktr* (which resembles *Trk* in many ways), and *Kdp* [47]. As shown in Figs. 5(a) and (b), three important genes of *Trk* system (*trkA*, *trkG*, and *trkH*) and four genes of *Kdp* system (*kdpA*, *kdpC*, *kdpD*, and *kdpE*) were downregulated at 5 g·L^{-1} ammonia compared with the control. The genes of K^+ efflux system (*kefB*, *kefC*, *kefF*, and *kefG*) were also decreased to low abundances. In addition, ion channel genes,

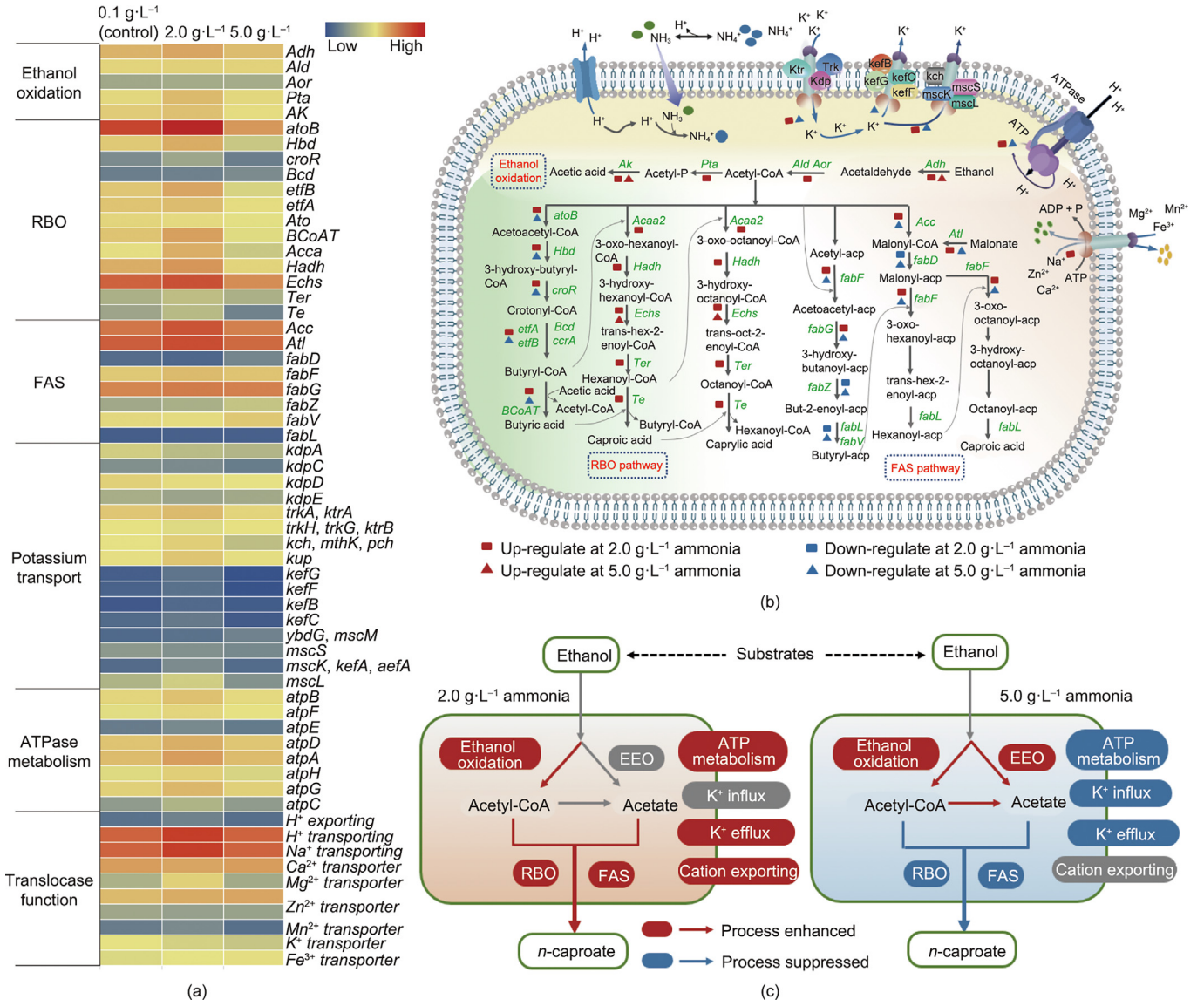

Fig. 5. Microbial *n*-caproate synthesis and metabolism related functions affected by different ammonia concentrations. (a) Heatmap for the relative abundances of functional genes and pathways; (b) the relevant functions up-regulated or down-regulated; (c) an overview of key processes in the ammonia-differentiated reactors. The icons on the right of Fig. 5(a) refer to the functional genes encoding *Adh*: alcohol dehydrogenase; *Ald*: aldehyde dehydrogenase; *Aor*: the aldehyde–ferredoxin oxidoreductase; *Pta*: phosphotransacetylase; *Ak*: acetate kinase; *atoB*: acetyl-CoA C-acetyltransferase; *Hbd*: 3-hydroxybutyryl-CoA dehydrogenase; *croR*: 3-hydroxybutyryl-CoA dehydratase; *Bcd*: butyryl-CoA dehydrogenase; *etfB*: electron transport flavoproteins beta subunit; *etfA*: electron transport flavoproteins alpha subunit; *Ato*: acetate CoA-transferase; *BCoAT*: butyryl-CoA: acetate CoA transferase; *Acca*: acetyl-CoA acyltransferase-2; *Hadh*: 3-hydroxyacyl-CoA dehydrogenase; *Echs*: enoyl-CoA hydratase; *Ter*: trans-2-enoyl-CoA reductase; *Te*: acyl-CoA thioesterase; *Acc*: acetyl-CoA carboxylase; *Atl*: acid-thiol ligases; *fabD*: phosphate butyryltransferase; *fabF*: β-ketoacyl-synthase Ⅱ; *fabG*: 3-oxoacyl-reductase; *fabZ*: 3-hydroxyacyl-dehydratase; *fabV*: enoyl-reductase; *fabL*: enoyl-[acyl-carrier-protein] reductase; *kdp*: potassium transport system; *kdpA*, *kdpC*, *kpdD*, and *kdpE*: potassium transporting P-type adenosine triphosphatase (ATPase) subunits A, C, D, and E; *trkA*, *ktrA*, *ktrB*, *trkG*, and *trkH*: potassium uptake protein; *mthK*: calcium-gated potassium channel; *pch* and *kch*: voltage-gated potassium channel; *kup*: K^+ uptake protein; *kefB*: glutathione-regulated potassium-efflux system protein; *kefC*, *kefF*, and *kefG*: glutathione-regulated potassium-efflux system ancillary protein; *ybdG* and *mscM*: miniconductance mechanosensitive (ms) channel; *mscK* and *kefA*: potassium-dependent ms channels; *aefA*: potassium-dependent ms channel; *mscS*: ms channels of small; *mscL*: ms channels of large; *atpA–H*: gene sequences encoding eight subunits of the ATP synthase; *ccrA*: crotonyl-CoA carboxylase/reductase; *Acaa2*: acetyl-CoA acyltransferase 2; acp: acyl carrier protein; ADP: adenosine diphosphate; FAS: fatty acid synthesis.

including genes encoding K^+ channels (*kch*), K^+-dependent mechanosensitive (ms) channels (*mscK*), and nonspecific ms channels including ms channels of miniconductance (*mscM*), small (*mscS*), and large (*mscL*) were reduced or almost unchanged at 5 g·L^{-1} ammonia. The downregulated genes of both K^+ influx and efflux systems suggested that the potassium transport function was suppressed by excessive ammonia, which weakened the ability of the cells to resist intracellular pH disturbance and proton imbalance. In comparison, the abundance of genes *trkA*, K^+ uptake protein (*kup*), *kch*, *mscK*, *mscL*, and *mscM* improved by > 30% under 2 g·L^{-1} ammonia. Although both K^+ influx and efflux were strengthened, more K^+ efflux functional genes were upregulated, which enabled the cells to pump out K^+ to resist ammonia toxicity.

(5) **Adenosine triphosphatase (ATPase) metabolism-related functions**. As discussed above, K^+ efflux, an energy-consuming process, changes under ammonia stress. The effects of ammonia on ATPase metabolism were analyzed to clarify the mechanism underlying ammonia inhibition.

Bacteria primarily express F-type ATPases that catalyze the conversion of adenosine diphosphate (ADP) to ATP [43]. The relative abundance of the F-type ATPase gene showed an 18.5% increase and a 4.3% decline compared to the control at 2 and 5 g·L^{-1} ammonia, respectively. Considering the strengthened K^+ efflux function, the increased ATPase gene expression at 2 g·L^{-1} ammonia ensured sufficient energy for K^+ efflux and other enzymatic reactions, exempting the damage to ammonia. However, K^+ efflux for the proton/pH balance and other metabolic reactions, including *n*-caproate generation, could be seriously blocked because of the decreased ATP harvest under high ammonia stress.

(6) **Translocase-related function.** Translocase is the seventh enzyme used to catalyze the transport of ions/molecules across the cell membrane or their translocation within the cell membrane. The abundance of the gene encoding translocases, especially the metal cation translocase, was significantly affected by ammonia content. In particular, the abundance of genes encoding Na^+, Ca^{2+}, and Zn^{2+}-exporting transporters was upregulated considerably under 2 g·L^{-1} ammonia, but was almost unchanged under 5 g·L^{-1} ammonia, consistent with the variations in genes encoding H^+-exporting transporters and H^+-transporting ATPases. This further supports the conclusion that metal cation and H^+ export would be promoted by energy consumption to alleviate ammonia toxicity, even below the ammonia inhibitory threshold. However, excessive ammonia can limit these detoxification behaviors. Moreover, genes for importing metal cations, including Mg^{2+}, Zn^{2+}, Mn^{2+}, Fe^{3+}, and K^+, were slightly downregulated under excessive ammonia. Zn^{2+} is the essential site for *Adh* and *Ald*, which catalyze ethanol oxidation. Fe^{2+} constitutes ferredoxin oxidoreductase, which plays a vital role in conserving CE energy [48]. The reduction in the import of metal cations could also be interpreted as a form of ammonia detoxification aimed at maintaining intracellular proton equilibrium. However, this simultaneously curtails the synthesis of metal-containing enzymes that are instrumental in *n*-caproate production.

An overview of the key processes promoted and inhibited in the ammonia-differentiated reactors is depicted in Fig. 5(c). In conclusion, functions including RBO, FAS, K^+ efflux, ATPase metabolism, and metal cation export were upregulated to some degree under the optimal ammonia content, which directly contributed to high *n*-caproate production. Except for metal cation export, other functions and K^+ influx were suppressed. The competing EEO process is promoted by excessive ammonia, indicating the loss of ammonia detoxification ability and the decline of other intracellular metabolic functions, including *n*-caproate synthesis.

4. Conclusions

This study evaluated the effects of ammonia on open-culture *n*-caproate production using ethanol as an electron donor, and comprehensively elucidated the underlying mechanism. The results revealed a progressive enhancement in both *n*-caproate yield and selectivity as the concentration of ammonia escalated from 0.1 to 2 g·L^{-1}. However, *n*-caproate production was significantly inhibited when the ammonia levels exceeded the threshold of 2 g·L^{-1}. Consequently, the optimal ammonia concentration and inhibitory threshold were determined to be 2 g·L^{-1}. Upon surpassing the inhibitory threshold, both FA and NH_4^+ contributed to inhibitory effects. Intriguingly, while ethanol oxidation remained largely unaffected, the excessive ammonia facilitated the competing EEO reaction and concurrently stifled the RBO pathway. This conclusion was supported by changes in key enzyme activities in these reactions. In addition, ammonia significantly affects the microbial community and function. More ammonia-tolerant CE-related bacteria were enriched, and functions, including RBO, FAS, K^+ efflux, ATPase metabolism, and metal cation export, were upregulated under the optimal ammonia concentration. In contrast, excessive ammonia led to the gradual disappearance of the CE functional bacteria. Simultaneously, the predominant functions involved in ammonia detoxification and *n*-caproate synthesis were notably suppressed by excessive ammonia. Therefore, controlling the ammonia concentration in *n*-caproate producing reactors is essential.

Acknowledgments

This work was supported by the Natural Science Foundation of Sichuan Province (2022NSFSC1042), the National Natural Science Foundation of China (52000132), and the Open Project of the State Key Laboratory of Urban Water Resource and Environment (Grant HC202241).

Compliance with ethics guidelines

Qing-Lian Wu, Ke-Xin Yuan, Wei-Tong Ren, Lin Deng, Hua-Zhe Wang, Xiao-Chi Feng, He-Shan Zheng, Nan-Qi Ren, and Wan-Qian Guo declare that they have no conflict of interest or financial conflicts to disclose.

Appendix A. Supplementary material

Supplementary data to this article can be found online at https://doi.org/10.1016/j.eng.2023.08.018.

References

[1] Wu Q, Bao X, Guo W, Wang B, Li Y, Luo H, et al. Medium chain carboxylic acids production from waste biomass: current advances and perspectives. Biotechnol Adv 2019;37(5):599–615.
[2] Chu N, Hao W, Wu Q, Liang Q, Jiang Y, Liang P, et al. Microbial electrosynthesis for producing medium chain fatty acids. Engineering 2022;16:141–53.
[3] Wu Q, Jiang Y, Chen Y, Liu M, Bao X, Guo W. Opportunities and challenges in microbial medium chain fatty acids production from waste biomass. Bioresour Technol 2021;340:125633.
[4] Angenent LT, Richter H, Buckel W, Spirito CM, Steinbusch KJJ, Plugge CM, et al. Chain elongation with reactor microbiomes: open-culture biotechnology to produce biochemicals. Environ Sci Technol 2016;50(6):2796–810.
[5] Choi K, Jeon BS, Kim BC, Oh MK, Um Y, Sang BI. *In situ* biphasic extractive fermentation for hexanoic acid production from sucrose by *Megasphaera elsdenii* NCIMB 702410. Appl Biochem Biotechnol 2013;171(5):1094–107.
[6] Levy PF, Sanderson JE, Cheng LK. Kolbe electrolysis of mixtures of aliphatic organic acids. J Electrochem Soc 1984;131(4):773–7.
[7] Harvey BG, Meylemans HA. 1-hexene: a renewable C6 platform for full-performance jet and diesel fuels. Green Chem 2014;16(2):770–6.
[8] De Leeuw KD, Buisman CJN, Strik DPBTB. Branched medium chain fatty acids: iso-caproate formation from iso-butyrate broadens the product spectrum for microbial chain elongation. Environ Sci Technol 2019;53(13):7704–13.
[9] Wu Q, Guo W, Bao X, Meng X, Yin R, Du J, et al. Upgrading liquor-making wastewater into medium chain fatty acid: insights into co-electron donors, key microflora, and energy harvest. Water Res 2018;145:650–9.
[10] Zhu X, Tao Y, Liang C, Li X, Wei N, Zhang W, et al. The synthesis of *n*-caproate from lactate: a new efficient process for medium-chain carboxylates production. Sci Rep 2015;5:14360.
[11] Grootscholten TIM, Strik DPBTB, Steinbusch KJJ, Buisman CJN, Hamelers HVM. Two-stage medium chain fatty acid (MCFA) production from municipal solid waste and ethanol. Appl Energy 2014;116:223–9.
[12] Wu Q, Feng X, Chen Y, Liu M, Bao X. Continuous medium chain carboxylic acids production from excess sludge by granular chain-elongation process. J Hazard Mater 2021;402:123471.
[13] Zhang W, Yin F, Dong H, Cao Q, Wang S, Xu J, et al. Bioconversion of swine manure into high-value products of medium chain fatty acids. Waste Manage 2020;113:478–87.
[14] Wang H, Zhang Y, Angelidaki I. Ammonia inhibition on hydrogen enriched anaerobic digestion of manure under mesophilic and thermophilic conditions. Water Res 2016;105:314–9.
[15] Vasudevan D, Richter H, Angenent LT. Upgrading dilute ethanol from syngas fermentation to *n*-caproate with reactor microbiomes. Bioresour Technol 2014;151:378–82.

[16] Weimer PJ, Nerdahl M, Brandl DJ. Production of medium-chain volatile fatty acids by mixed ruminal microorganisms is enhanced by ethanol in co-culture with *Clostridium kluyveri*. Bioresour Technol 2015;175:97–101.
[17] Zhang C, Yang L, Tsapekos P, Zhang Y, Angelidaki I. Immobilization of *Clostridium kluyveri* on wheat straw to alleviate ammonia inhibition during chain elongation for *n*-caproate production. Environ Int 2019;127:134–41.
[18] Wei Y, Ren B, Zheng S, Feng X, He Y, Zhu X, et al. Effect of high concentration of ammonium on production of *n*-caproate: recovery of a high-value biochemical from food waste via lactate-driven chain elongation. Waste Manage 2021;128:25–35.
[19] Liu T, Sung S. Ammonia inhibition on thermophilic aceticlastic methanogens. Water Sci Technol 2002;45(10):113–20.
[20] Wang Z, Chen M, Xu Y, Li S, Lu W, Ping S, et al. An ethanol-tolerant recombinant *Escherichia coli* expressing *Zymomonas mobilis pdc* and *adhB* genes for enhanced ethanol production from xylose. Biotechnol Lett 2008;30 (4):657–63.
[21] Luo J, Feng L, Chen Y, Sun H, Shen Q, Li X, et al. Alkyl polyglucose enhancing propionic acid enriched short-chain fatty acids production during anaerobic treatment of waste activated sludge and mechanisms. Water Res 2015;73:332–41.
[22] Castao-Cerezo S, Bernal V, Rhrig T, Termeer S, Cánovas M. Regulation of acetate metabolism in *Escherichia coli* BL21 by protein N^{ε}-lysine acetylation. Appl Microbiol Biotechnol 2015;99(8):3533–45.
[23] Zhu X, Zhou Y, Wang Y, Wu T, Li X, Li D, et al. Production of high-concentration *n*-caproic acid from lactate through fermentation using a newly isolated *Ruminococcaceae* bacterium CPB6. Biotechnol Biofuels 2017;10:102.
[24] Anthonisen AC, Loehr RC, Prakasam TBS, Srinath EG. Inhibition of nitrification by ammonia and nitrous acid. J Water Pollut Control Fed 1976;48(5):835–52.
[25] Roghair M, Hoogstad T, Strik DPBTB, Plugge CM, Timmers PHA, Weusthuis RA, et al. Controlling ethanol use in chain elongation by CO_2 loading rate. Environ Sci Technol 2018;52(3):1496–505.
[26] Chen JL, Ortiz R, Steele TWJ, Stuckey DC. Toxicants inhibiting anaerobic digestion: a review. Biotechnol Adv 2014;32(8):1523–34.
[27] Calli B, Mertoglu B, Inanc B, Yenigun O. Effects of high free ammonia concentrations on the performances of anaerobic bioreactors. Process Biochem 2005;40(3,4):1285–92.
[28] Shi X, Lin J, Zuo J, Li P, Li X, Guo X. Effects of free ammonia on volatile fatty acid accumulation and process performance in the anaerobic digestion of two typical bio-wastes. J Environ Sci 2017;55:49–57.
[29] El Hadj TB, Astals S, Gali A, Mace S, Mata-Álvarez J. Ammonia influence in anaerobic digestion of OFMSW. Water Sci Technol 2009;59(6):1153–8.
[30] Ma H, Wu W, Yu Z, Zhao J, Fu P, Xia C, et al. Medium-chain fatty acid production from Chinese liquor brewing yellow water by electro-fermentation: division of fermentation process and segmented electrical stimulation. Bioresour Technol 2022;360:127510.
[31] Coma M, Vilchez-Vargas R, Roume H, Jauregui R, Pieper DH, Rabaey K. Product diversity linked to substrate usage in chain elongation by mixed-culture fermentation. Environ Sci Technol 2016;50(12):6467–76.
[32] Rabelo CABS, Okino CH, Sakamoto IK, Varesche MBA. Isolation of *Paraclostridium* CR4 from sugarcane bagasse and its evaluation in the bioconversion of lignocellulosic feedstock into hydrogen by monitoring cellulase gene expression. Sci Total Environ 2020;715:136868.
[33] Zagrodnik R, Duber A, Łężyk M, Oleskowicz-Popiel P. Enrichment versus bioaugmentation—microbiological production of caproate from mixed carbon sources by mixed bacterial culture and *Clostridium kluyveri*. Environ Sci Technol 2020;54(9):5864–73.
[34] Yin Y, Wang J. Enhanced medium-chain fatty acids production from Cephalosporin C antibiotic fermentation residues by ionizing radiation pretreatment. J Hazard Mater 2022;440:129714.
[35] Jiang X, Lyu Q, Bi L, Liu Y, Xie Y, Ji G, et al. Improvement of sewage sludge anaerobic digestion through synergistic effect combined trace elements enhancer with enzyme pretreatment and microbial community response. Chemosphere 2022;286(Pt 1):131356.
[36] Lu Y, Yuan H, Yan B, Zuo X, Li X. Improved performance of corn stover anaerobic digestion by low-temperature hydrothermal pretreatment with urea enhancement. Biomass Bioenergy 2022;164:106553.
[37] She Y, Hong J, Zhang Q, Chen BY, Wei W, Xin X. Revealing microbial mechanism associated with volatile fatty acids production in anaerobic acidogenesis of waste activated sludge enhanced by freezing/thawing pretreatment. Bioresour Technol 2020;302:122869.
[38] Ma H, Yu Z, Wu W, Fu P, Xia C, Lam SS, et al. Effects of ethanol addition on caproic acid production and rumen microorganism community structure from straw fermentation. Fuel 2022;327:125142.
[39] Zhang Y, Pan X, Zuo J, Hu J. Production of *n*-caproate using food waste through thermophilic fermentation without addition of external electron donors. Bioresour Technol 2022;343:126144.
[40] Qian DK, Geng ZQ, Sun T, Dai K, Zhang W, Zeng RJ, et al. Caproate production from xylose by mesophilic mixed culture fermentation. Bioresour Technol 2020;308:123318.
[41] Dang Y, Holmes DE, Zhao Z, Woodard TL, Zhang Y, Sun D, et al. Enhancing anaerobic digestion of complex organic waste with carbon-based conductive materials. Bioresour Technol 2016;220:516–22.
[42] Duan X, Chen Y, Feng L, Zhou Q. Metagenomic analysis reveals nonylphenol-shaped acidification and methanogenesis during sludge anaerobic digestion. Water Res 2021;196:117004.
[43] Xing L, Ma J, Yin Q, Wu G. Metagenomic analysis reveals the methanogenic, ATP, and potassium-transport metabolisms of anaerobic systems with different ammonia concentrations. Sci Total Environ 2021;782:146911.
[44] Seedorf H, Fricke WF, Veith B, Brüggemann H, Liesegang H, Strittmatter A, et al. The genome of *Clostridium kluyveri*, a strict anaerobe with unique metabolic features. Proc Natl Acad Sci USA 2008;105(6):2128–33.
[45] Han W, He P, Shao L, Lü F. Metabolic interactions of a chain elongation microbiome. Appl Environ Microbiol 2018;84(22):e01614–e1618.
[46] Yan M, Treu L, Zhu X, Tian H, Basile A, Fotidis IA, et al. Insights into ammonia adaptation and methanogenic precursor oxidation by genome-centric analysis. Environ Sci Technol 2020;54(19):12568–82.
[47] Epstein W. The roles and regulation of potassium in bacteria. Prog Nucleic Acid Res Mol Biol 2003;75:293–320.
[48] Fu X, Jin X, Ye R, Lu W. Nano zero-valent iron: a pH buffer, electron donor and activator for chain elongation. Bioresour Technol 2021;329:124899.